Strategies to Improve Photostabilities in Ultrasensitive Fluorescence Spectroscopy

Jerker Widengren,*,† Andriy Chmyrov,† Christian Eggeling,‡ Per-Åke Löfdahl,†,§ and Claus A. M. Seidel||

Experimental Biomolecular Physics, Department of Applied Physics, Albanova University Center, Royal Institute of Technology, SE-10691 Stockholm, Sweden, Max-Planck-Institut für Biophysikalische Chemie, Am Fassberg 11, D-37077 Göttingen, Germany, and Institut für Physikalische Chemie, Heinrich-Heine Universität, D-40225 Düsseldorf, Germany

Received: July 21, 2006; In Final Form: October 10, 2006

Given the particular importance of dye photostability for single-molecule and fluorescence fluctuation spectroscopy investigations, refined strategies were explored for how to chemically retard dye photobleaching. These strategies will be useful for fluorescence correlation spectroscopy (FCS), fluorescence-based confocal single-molecule detection (SMD) and related techniques. In particular, the effects on the addition of two main categories of antifading compounds, antioxidants (*n*-propyl gallate, nPG, ascorbic acid, AA) and triplet state quenchers (mercaptoethylamine, MEA, cyclo-octatetraene, COT), were investigated, and the relevant rate parameters involved were determined for the dye Rhodamine 6G. Addition of each of the compound categories resulted in significant improvements in the fluorescence brightness of the monitored fluorescent molecules in FCS measurements. For antioxidants, we identify the balance between reduction of photoionized fluorophores on the one hand and that of intact fluorophores on the other as an important guideline for what concentrations to be added for optimal fluorescence generation in FCS and SMD experiments. For nPG/AA, this optimal concentration was found to be in the lower micromolar range, which is considerably less than what has previously been suggested. Also, for MEA, which is a compound known as a triplet state quencher, it is eventually its antioxidative properties and the balance between reduction of fluorophore cation radicals and that of intact fluorophores that defines the optimal added concentration. Interestingly, in this optimal concentration range the triplet state quenching is still far from sufficient to fully minimize the triplet populations. We identify photoionization as the main mechanism of photobleaching within typical transit times of fluorescent molecules through the detection volume in a confocal FCS or SMD instrument ($<1-20$ ms), and demonstrate its generation via both one- and multistep excitation processes. Apart from reflecting a major pathway for photobleaching, our results also suggest the exploitation of the photoinduced ionization and the subsequent reduction by antioxidants for biomolecular monitoring purposes and as a possible switching mechanism with applications in high-resolution microscopy.

1. Introduction

Photophysical and photochemical properties of fluorescent marker molecules are of great importance for all applications of fluorescence spectroscopy where a high read-out rate or a high sensitivity is required. In particular, this is important for applications regarding single-molecule detection (SMD) or fluorescence correlation spectroscopy (FCS) in which a low fluorescence signal cannot be compensated by an increased fluorophore concentration. In this respect, there is a need to optimize the fluorescence, both with respect to the total number of photons that can be extracted per molecule as well as with respect to the fluorescence emission rate itself. Chemically, different strategies have been proposed for how to improve the fluorescence rate and decrease photobleaching including deoxygenation and addition of antioxidants, oxygen scavengers, singlet oxygen quenchers, or triplet state quenchers.[1] However, for compounds having a retarding effect on the bleaching of fluorophores (expressed as the bleaching probability per excitation cycle or the photodegradation rate given a certain excitation intensity), a corresponding or even stronger fluorescence quenching often occurs.[2−5] As a consequence, bleaching retardation by fluorescence quenching can indeed maintain a certain fluorescence intensity level from a sample over a longer time, but the total amount of emitted fluorescence photons from the sample will not increase. This mechanism therefore does not provide a true strategy to retard photobleaching itself, and in particular for SMD and FCS experiments it will not prove useful given the importance of the fluorescence emission rate per molecule as a figure of merit. In addition, for many compounds the reported antibleaching effects have often been found to be contradictive for one and the same compound.[6,7] This can partly be rationalized to be an effect of differences in the environments under which the different investigations were made. However, it may also reflect that the underlying mechanisms of photobleaching are not fully understood, and that much of the data on photophysical parameters of fluorophores can be inconsistent or vary considerably between different reports[8,9] or with dye concentration levels.[5,10] Moreover, not only the environment and

* Corresponding author. Telephone: +46-8-55378030. Fax: +46-8-55378216. Email: jerker@biomolphysics.kth.se

† Royal Institute of Technology.

‡ Max-Planck-Institut für Biophysikalische Chemie.

§ Present address: Dept. Biotechnology, Royal Institute of Technology, SE-10691 Stockholm, Sweden.

|| Heinrich-Heine Universität.

10.1021/jp0646325 CCC: $37.00
Published on Web 12/29/2006

concentration of fluorophores but also the excitation conditions can have a substantial effect on the bleaching properties.[9,11−13] Therefore, one should not expect a photostability of a certain dye at a certain concentration in a certain environment investigated within a conventional fluorescence ensemble experiment to be fully comparable to the photostability it would have in a SMD or a FCS experiment in which the excitation rate is typically considerably higher.

In previous works, it has been shown how FCS itself can be used as a method to characterize fluorophores on a microscopic scale with respect to fluorescence saturation involving triplet state formation,[8,14] charge transfer,[15] isomerization,[16] and photodegradation,[9,12] providing a useful alternative and complementary technique to previously more established photophysical techniques such as flash photolysis. In this work, we have used FCS to study the impact of different antifading compounds with a particular focus on excitation conditions relevant for fluorescence-based confocal SMD and fluctuation spectroscopy. The purpose is to better define mechanisms and useful concentration levels of suitable additives and thereby refine strategies for how to chemically retard dye photobleaching under conditions relevant for SMD, FCS, and related techniques.

The strong dependence on both environmental and excitation conditions indicate that photobleaching can occur by several different mechanisms and, from a general point of view, can be considered to be quite complex.[17] However, the mechanisms that are maybe the most often referred to and of strongest relevance are (*i*) photo-oxidation in which chemically reactive singlet oxygen is formed by sensitization of ground-state triplet oxygen molecules by triplet state dyes,[18,19] and (*ii*) photoionization, taking place on the basis that the dye molecules in polar solvents after excitation to the first or higher excited electronic states more efficiently generate highly reactive radicals and solvated electrons.[9,12,13,20,21] Removal of oxygen has been proposed as a remedy against photobleaching by photo-oxidation. On the other hand, interaction of oxygen with dyes in their metastable states such as the triplet state can lead to both ground state recovery and generation of irreversible photoproducts. Thus, depending on which effect is predominantly suppressed, deoxygenation has been found to decrease,[4,17,22,23] even increase,[9,24] or to leave the photobleaching quantum yield mainly unaffected.[25−27] In this study, we instead concentrated our efforts to investigating the effects on the addition of two main categories of antifading compounds: antioxidants, possibly promoting recovery of photoionized dye radicals, and triplet state quenchers, by which generation of singlet oxygen also should be reduced.

Among antioxidants, we focused on *n*-propyl gallate (nPG) and ascorbic acid (AA). Retarding effects on photobleaching when adding nPG up to concentrations of 10 mM have been reported for fluorescein conjugates in glycerol,[2,28] in aqueous solution,[29] and for phycobiliproteins in phosphate buffer.[27] nPG has well-known antioxidative properties and is also used to prevent oxidative deterioration of fatty materials such as edible oils and fats as well as cosmetic products.[30,31] Likewise, the antioxidative effects of AA (vitamin C) have been well-known for a long time. In many different organisms, AA is one of the main intracellular antioxidants[32] and is also widely used as a food preservative.[33] In fluorescence spectroscopy, AA has been used as a radical scavenger and antioxidant with a reported retarding effect on the photobleaching rates.[26,34−37]

By many investigators, the triplet state is considered to be the main precursor state of photobleaching. For this reason, it is of interest to find triplet state quenchers that ideally would improve the fluorescence rate as well as retard photobleaching. Here, we study the effects of mercaptoethylamine (MEA) in water and cyclo-octatetraene (COT) in ethanol. In the past, the addition of triplet state quenchers has proven to be a useful strategy to improve both outcome of fluorescence spectroscopic studies[5,36,37] as well as performance of dye lasers.[38−41]

In the framework of single-molecule and fluctuation spectroscopy, our investigations indicate that the impact of the additives is sometimes different from what has previously been reported in conventional fluorescence ensemble studies. Their mechanisms of action are investigated and the relevant rate parameters involved are determined.

2. Experimental Setup

The experimental setup for the FCS studies has been previously described.[9,12,14,42] The fluorophore molecules under investigation were illuminated through a microscope cover glass-corrected water-immersion objective (Zeiss, Plan-Neofluar, 63x, 1.2 N.A., 160 mm tube length) by a strongly focused beam (diameter 0.6 μm) of an argon-ion laser (Spectra Physics 165, 514 nm emission wavelength). The fluorescent light was collected by the same objective and was detected by two avalanche photodiodes (EG&G/Perkin-Elmer) in a beam splitting arrangement. Typical diffusion times of the fluorophores through the detection volume were 40−50 μs at room temperature (21 ± 3 °C). By use of the two detectors, all inherent noise due to the detectors alone, as well as their dead times, can be eliminated as long as it is not correlated between the detectors. A band-pass filter (Omega Optics 565DF50) was inserted in front of the detectors, and a pinhole (30 μm diameter) was placed in the image plane to discriminate the fluorescence spectrally and spatially, respectively. The signals of the two detectors were transferred to a PC-based correlator (ALV-5000 with fast option). Rhodamine 6G (Rh6G) (Lambda Physik) was dissolved in ethanol and was diluted to nanomolar concentrations in ultrapure water or ethanol. MEA, COT, nPG, and AA (Sigma Chemicals) were then added without further purification. Solutions were prepared freshly in direct conjunction to the experiments to minimize oxidative deterioration.

By defocusing the excitation laser beam (diameter 3 μm in focus) and by inserting a larger pinhole (200 μm in diameter), an increased excitation/detection volume was obtained in the FCS measurements. With this arrangement, typical dwell times of the fluorophores within the detection volume were increased to 2.2−2.5 ms, allowing transient states with relaxation times up to this time range to be analyzed. Complementary measurements with an expanded detection volume were also performed at a separate setup (diffusion time 1.1−1.3 ms, laser beam diameter in focus 2 μm, pinhole 150 μm) based on a similar instrumentation (objective: Olympus 60x, NA 1.2). The measured correlation curves were fitted to different expressions for the FCS curves as stated, using a Levenberg−Marquardt nonlinear least-squares algorithm.[43]

3. Theoretical Background

In FCS, the fluorescence intensity fluctuations of fluorescent molecules excited by a focused laser beam are studied.[44−46] A broad range of dynamic processes can be analyzed as long as they reflect themselves in terms of fluorescence fluctuations. Typically, fluorescence fluctuations arise as a result of translational diffusion of the fluorescent molecules into and out of the sample volume element and from transitions to and from the triplet states of the fluorophores. The time dependent part of the correlation function can then be expressed as[8]

$$G(\tau) = \frac{1}{N(1 - T_{1eq})}\left(\frac{1}{1 + \tau/\tau_D}\right)\left(\frac{1}{1 + (\omega_0/\omega_z)^2(\tau/\tau_D)}\right)^{1/2} \times [1 - T_{1eq} + T_{1eq}\exp(-\tau/\tau_T)] \quad (1)$$

Here, N is the mean number of fluorescent molecules within the sample volume element. ω_0 and ω_z are the distances from the center of the laser beam focus in the radial and axial direction respectively at which the collected fluorescence intensity has dropped by a factor of e^2 compared to its peak value. The sample volume element is determined by the spatial distribution of the laser excitation and the collection efficiency function in the confocal setup. The characteristic diffusion time for the fluorescent molecules is given via the diffusion coefficient, D, by $\tau_D = \omega_0^2/4D$. Equation 1 assumes the collected fluorescence to be Gaussian shaped in the axial as well as in the radial direction but, under our conditions, also provides a good approximation for the case of a Lorentzian-shaped axial profile of the laser beam.[42] T_{1eq} is the mean fraction of fluorophores within the sample volume element being in their triplet states and τ_T is the relaxation time related to the triplet state relaxation. Making the simplifying assumption of a uniform excitation profile within the detection volume, the expressions for τ_T and T_{1eq} are given by[12,14]

$$1/\tau_T = k_T + \frac{\sigma_{01}I_{exc}k_{ISC}}{k_{10} + \sigma_{01}I_{exc}} \quad (2)$$

$$T_{1eq} = \frac{\sigma_{01}I_{exc}k_{ISC}}{\sigma_{01}I_{exc}(k_T + k_{ISC}) + k_{10}k_T} \quad (3)$$

Here, with reference to the simple three-state model of Figure 1, k_{10} is the deactivation rate of the first excited singlet state, S_1, to the ground singlet state, S_0. k_{ISC} denotes the rate of intersystem crossing from S_1 to the lowest triplet state, T_1. k_T is the rate of triplet state deactivation from T_1 to S_0, σ_{01} is the excitation cross section, I_{exc} signifies the average excitation intensity within the detection volume, and the average excitation rate within the detection volume then given by $k_{01} = \sigma_{01}I_{exc}$.

Effects of termination of fluorescence emission of dye molecules during their passage through the volume element has experimentally been shown to result in an additional factor to the correlation function of eq 1:[9,12]

$$G_B(\tau) = G(\tau)(1 - B + B\exp(-k_B\tau)) \quad (4)$$

The decrease in the time the molecules remain fluorescent while passing the sample volume caused by photobleaching thus results in a shortening of the overall decay time of the correlation curves. Because photobleaching occurs only in the irradiated volume element, typically comprising only a small fraction of the total sample volume, an exchange of photodestructed to intact dye molecules takes place during measurements. Therefore, unless the total sample volume (i.e., the space within which the fluorescent molecules are free to diffuse) is not further restricted,[47,48] and following a possible initial equilibration after onset of excitation, a close to steady-state concentration of intact fluorescent molecules can be maintained in the detection volume. This makes it possible to treat the photobleaching reaction as a chemical pseudo-equilibrium reaction with the effective rate constant for bleaching k_B, and B specifying the average fraction of fluorophores undergoing photobleaching within their passages through the detection volume. At first glance, B would be expected to be equal to 1. However, typically this is not the case. This can largely be attributed to a nonuniform excitation profile and different diffusion pathways through the detection volume, leading to different excitation histories of the interrogated molecules. One contributing reason can also be that not all molecules are subject to the same photobleaching pathways. Under our conditions, and by assuming an average photobleaching rate constant, the actual space-dependent distribution of the bleaching reactions within the excitation volume can be shown to best correspond to an overall bleaching reaction with a uniform bleaching rate k_B affecting a fraction of about 0.8 of all the molecules contained in the detection volume.[12]

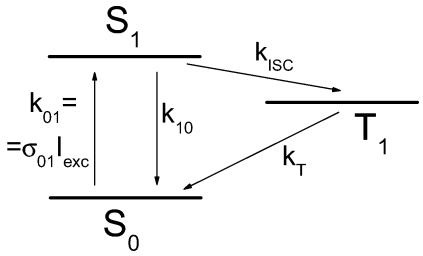

Figure 1. Simple photodynamic model including the three main states involved in singlet−triplet transitions of Rh6G molecules in aqueous solution (see text for details).

4. Results and Discussion

4.1 Addition of Antioxidants. *4.1.1. Millimolar concentrations of nPG in water.* We first investigated the possible retarding effect of nPG on the photobleaching of Rh6G in water. According to previous reports on the photobleaching retarding effects of nPG, relatively high nPG concentrations of around 10 mM should be necessary to obtain a significant effect.[2,28,29] However, from our FCS measurements, nPG was found to strongly quench the fluorescence of the Rh6G molecules at these concentrations. To analyze the nature of the quenching more closely, a series of correlation curves were measured at varying nPG concentrations (0.25−10 mM) and excitation intensities (20kW/cm^2−6MW/cm^2) (Figure 2). The measured fluorescence autocorrelation curves showed a characteristic decay in the time range of a few hundred nanoseconds or shorter, which very much resembled that obtained from the electron transfer induced quenching of deoxy guanosine triphosphate (dGTP) in a previous study.[15] The time-dependent part of the correlation curves could be well fitted to the expression of eq 1 with an additional exponential process included. Then, with $G_D(\tau)$ denoting the diffusion dependent part (2nd and 3rd factors) of $G(\tau)$ in eq. 1,

$$G(\tau) = \frac{1}{N(1 - T_{eq} - C_{eq})}G_D(\tau)[1 - T_{eq} - C_{eq} + T_{eq}\exp(-\tau/\tau_T) + C_{eq}\exp(-\tau/\tau_C)] \quad (5)$$

Similar to dGTP and because nPG is known as a reducing agent, this additional exponential process can be attributed to nPG acting as an electron donor with charge-transfer taking place upon hydrophobic interaction between the nPG and the Rh6G molecules. As for the charge transfer observed for Rh6G and dGTP,[15] a rate scheme as outlined in the inset of Figure 2 was used to describe the observed exponential relaxations in the FCS curves. This rate scheme includes the three state model of Rh6G with ground and first-excited singlet states, S_0 and S_1, and the lowest triplet state T_1, as depicted in Figure 1. It also includes the possibility of complex formation between Rh6G and nPG and subsequent electron transfer from nPG to Rh6G with different rates depending on if Rh6G is in its S_0 or S_1 state. The rate scheme can be reduced to a three state model,

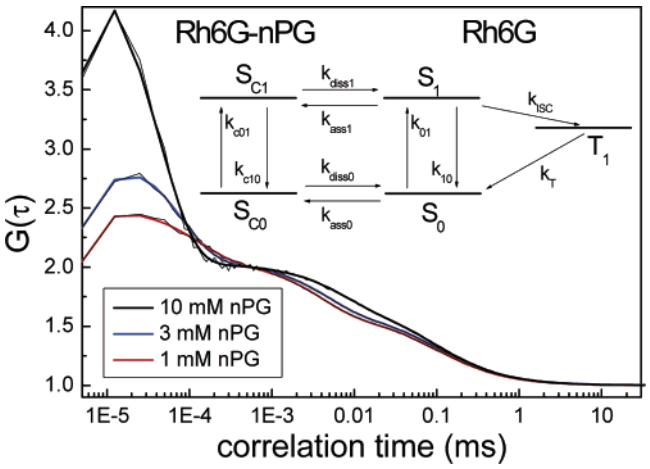

Figure 2. FCS curves of R6G in aqueous solution containing 1, 3, and 10 mM concentrations of nPG. Excitation intensity 4 MW/cm^2. Obtained relaxation parameters (C_{eq}/τ_C, T_{eq}/τ_T): 0.31/0.12 μs, 0.30/3.6 μs (1 mM), 0.49/0.079 μs, 0.20/4.7 μs (3 mM), 0.76/0.040 μs, 0.075/7.1 μs (10 mM). Inset: rate scheme describing the relaxation behavior of the two exponential processes of the recorded correlation curves, involving singlet−triplet transitions and charge transfer following hydrophobic complex formation (Rh6G−nPG), where k_{dissX} and k_{assX} refer to the rates of dissociation and association, respectively, between Rh6G and nPG with Rh6G in the excited ($X = 1$) or in the ground state ($X = 0$). The initial rise in the correlation curves is attributed to antibunching (arising from the population relaxation within the singlet entity following the S_0-S_1 excitation and the S_1-S_0 de-excitation). The amplitude of correlation curves are normalized to 1 at 0.5 μs (see text and ref 15 for further details).

consisting of a Rh6G singlet state, S (S_0 and S_1), the lowest triplet state, T_1, and a complexed state with nPG, C (S_{C0} and S_{C1}, denoting the ground and first-excited singlet states of Rh6G when in complex with nPG, see inset Figure 2), by recognizing that the intrasinglet state transitions (i.e., those between S_0 and S_1, and between S_{C0} and S_{C1}, respectively) take place on a time scale much faster than any of the other dynamic processes involved:

$$C \underset{k_{diss0}}{\overset{k_{ass}'}{\rightleftharpoons}} S \underset{k_T}{\overset{k_{ISC}'}{\rightleftharpoons}} T_1 \qquad (6)$$

Here, $k_{ass}' = k_{01}/(k_{01} + k_{10})k_{ass1} + k_{10}/(k_{01} + k_{10})k_{ass0}$ and $k_{ISC}' = k_{01}/(k_{01} + k_{10})k_{ISC}$ denote the effective rates of complex formation between Rh6G and nPG and of intersystem crossing within the Rh6G molecules, respectively. When Rh6G is in a complex state with nPG (C), the deactivation rate $k_{c10} \gg k_{10}$ and the population of S_{C1} is negligible (see inset Figure 2). Therefore, dissociation from S_{C1} via k_{diss1} can be disregarded in eq 6). The measured amplitudes (T_{eq} and C_{eq}) and relaxation times (τ_T and τ_C) from the correlation curves are given from the corresponding rate equations, i.e., from the following system of coupled first order differential equations

$$\frac{d}{dt}\begin{pmatrix} S \\ T_1 \\ C \end{pmatrix} = \begin{bmatrix} -(k_{ISC}' + k_{ass}') & k_T & k_{diss0} \\ k_{ISC}' & -k_T & 0 \\ k_{ass}' & 0 & -k_{diss0} \end{bmatrix}\begin{pmatrix} S \\ T_1 \\ C \end{pmatrix} \qquad (7)$$

by its steady-state populations of T_1 and C, and the inversed nonzero eigenvalues of its rate matrix, respectively (see ref 15 for further details). Consequently, the relaxation processes observed in the FCS curves and their amplitudes and relaxation times can be expressed as functions of the association rate coefficients for formation of nPG/Rh6G complexes from the ground and excited singlet states (k_{ass0} and k_{ass1}, respectively),

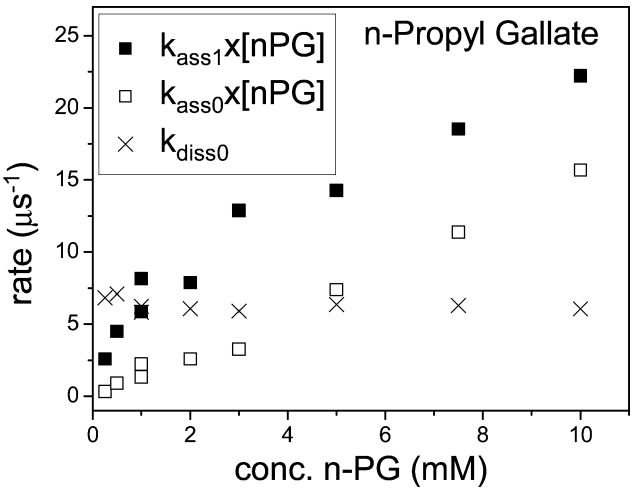

Figure 3. Calculated rates of association (k_{ass0}, k_{ass1}) and dissociation (k_{diss}) of Rh6G and nPG, obtained by global fitting of the relaxation rates and amplitudes of charge transfer (τ_C and C_{eq}) and singlet−triplet state transitions (τ_T and T_{eq}) observed in the FCS curves (Figure 2) for the given concentrations (see text and ref 15 for further details).

the dissociation rate of the hydrophobic complexes (k_{diss0}), and the triplet state parameters k_{ISC} and k_T. The excitation intensity and nPG concentration dependencies of the amplitudes T_{eq} and C_{eq} and the relaxation times τ_T and τ_C were analyzed in analogy to the procedure presented in ref 15. For each concentration of nPG, the rate coefficients k_{ass0}, k_{ass1}, k_{diss0}, k_{ISC}, and k_T were retrieved by global fitting of C_{eq}, T_{eq}, τ_T, and τ_C, measured at different excitation intensities (20kW/cm^2−6MW/cm^2) (see ref 15 for details).

The obtained rate constants of k_{ass0}, k_{ass1}, and k_{diss0} are plotted versus the concentration of nPG in Figure 3. For concentrations below a few millimolar, a close to linear relationship on [nPG] was found for k_{ass0} ($1.5 \pm 0.3 \times 10^9$ M^{-1} s^{-1}) and k_{ass1} ($5 \pm 2 \times 10^9$ M^{-1} s^{-1}), while k_{diss0} (6×10^6 s^{-1}) showed a close to constant value independent of [nPG]. The obtained parameter values are close to those found for dGTP and Rh6G.[15] For Rh6G/dGTP as well as for Rh6G/nPG, the partly hydrophobic nature of the molecules promotes aggregate formation and subsequent electron transfer to Rh6G. From the rate constants, we get the dissociation constants $K_{D0} = k_{ass0}/k_{diss0} = 250$ M^{-1}, and $K_{D1} = k_{ass1}/k_{diss0} = 830$ M^{-1}. These are about a factor of 2 higher than those for dGTP and indicate a slightly more hydrophobic character of nPG. The hydrophobic character (i.e., an increased tendency for dimer formation at higher nPG concentrations) is also a possible explanation for the slight deviation from linearity of the association rates over [nPG] as observed in particular for k_{ass1} in Figure 3. The triplet parameters k_T and k_{ISC} were found to be clearly reduced in the presence of nPG (down to 0.2×10^6 s^{-1} and 0.7×10^6 s^{-1} from 0.5×10^6 s^{-1} and 1.1×10^6 s^{-1} in the absence of nPG, respectively) and in particular for nPG concentrations in the upper range (2 mM−10 mM). We attribute these rate reductions to complex formation between Rh6G and nPG, a subsequent shielding of oxygen, and a reduced oxygen-induced enhancement of both k_T and k_{ISC}. Again, a similar effect was noticed for the interactions between Rh6G and dGTP, as previously reported.[15]

In other words, at millimolar concentrations nPG does not show an overall beneficial effect on the Rh6G fluorescence due to its strong contribution to both static (k_{ass0}) as well as dynamic (k_{ass1}) fluorescence quenching. Although the photobleaching measurements undertaken at those concentrations indeed show a retardation of the photobleaching, also under our conditions (no significant shortening of the overall decay times of the

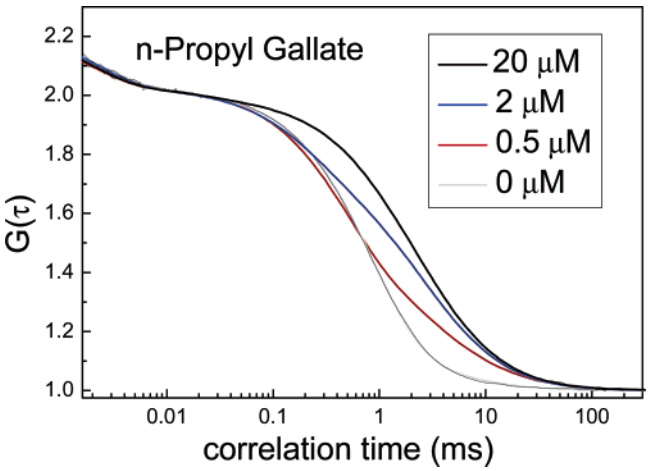

Figure 4. FCS curves recorded from Rh6G and nPG in aqueous solution using an expanded sample volume. nPG concentrations are between 0 and 20 micromolar. Excitation intensity 0.2 MW/cm^2. $\dot{R}^+$ and τ_R (replacing B and $1/k_B$, respectively in eq 4) values of the curves: 0.04/0.022 ms (20 μM), 0.22/0.21ms (20 μM), 0.47/0.49 ms (0.5 μM), 0.76/1.6 ms (0 μM). $T_{eq} = 0.16 \pm 0.01$ and $\tau_T = 2.3 \pm 0.4$ μs for all curves. The amplitude of correlation curves are normalized to 1 at 10 μs.

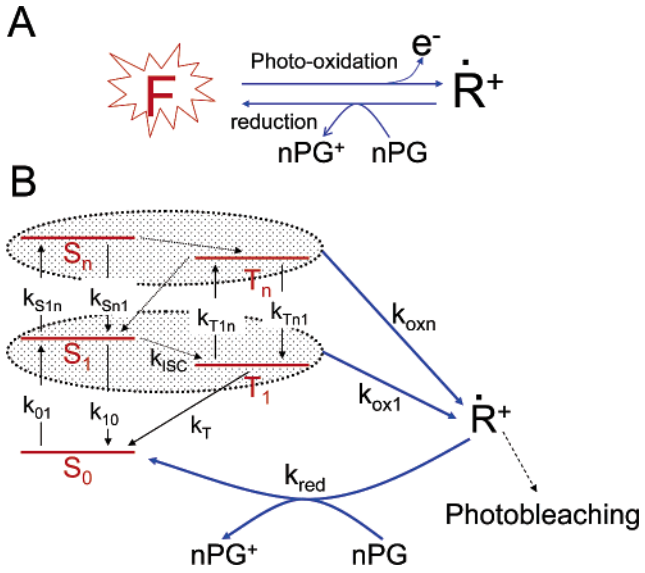

Figure 5. (A): Major features of the photoionization/reduction process of R6G in the prescence of nPG, viewed on a time scale $\gg$ the triplet relaxation time τ_T. F denotes the fluorescent, non-ionized fluorophore, $\dot{R}^+$ is the photoionized state that can be regenerated into F by donation of an electron from nPG. k_{ox}' and k_{red}' denote the effective rates of photo-oxidation and reduction by nPG, respectively. (B): Five-state model taking photoionization from both first and higher excited singlet (S_1 and S_n) and triplet states (T_1 and T_n) into account. k_{ox1} and k_{oxn} denote the rate coefficients for photo-oxidation from the lower and higher excited singlet/triplet states, respectively. See text for further details.

correlation curves) the fluorescence quenching is much more pronounced. Under our conditions, addition of nPG in millimolar concentrations therefore does not seem to provide a useful strategy to reduce photobleaching.

4.1.2. Micromolar Concentrations of nPG in Water. In contrast, at concentration levels of nPG in the μM range when most of the static and dynamic quenching effects observed at millimolar concentration were no longer traceable, the retarding effect of nPG was still pronounced in the sense that addition of increasing amounts of nPG increased the overall decay times of the correlation curves. In particular, this effect could clearly be seen from the FCS measurements when expanding the sample volume element so that the passage time of the Rh6G molecules were in the order of a few milliseconds (Figure 4). In this way, the exposure and interrogation time of the molecules passing the detection volume by diffusion is made longer, and any present influence of photobleaching is made more pronounced.

These correlation curves recorded with the expanded sample volume were found to be well fitted to the expression of eq 4. Thus, the relaxation times showed a behavior similar to that previously analyzed and attributed to photobleaching.[9,12] However, with increasing concentrations of nPG the amplitude B was found to continuously decrease, while the relaxation rate k_B was found to increase (Figure 4). Taking into account the ability of nPG to act as an electron donor, as shown above, this behavior is well in agreement with a bimolecular reaction involving the nPG and the fluorophore molecules. In this reaction, the fluorescence emission of the fluorophores can be "switched off" as a consequence of laser irradiation and photoionization. The photoionized Rh6G molecules can then be "switched on" again by receiving an electron, following a collisional encounter with an nPG molecule. The major features of this photoionization/reduction process are outlined in Figure 5a. From the relaxation times of the correlation curves of Figure 4, we note that the oxidation/reduction typically takes place on a time scale of 100 μs and longer. This is a much slower time scale than that of the transitions between the singlet states and the triplet state, which typically have relaxation times, τ_T, in the range of a few μs (at air-saturated conditions). We can therefore consider the singlet−triplet transitions to be equilibrated on the time scale of this oxidation/reduction of the fluorophores. The photoionization/reduction reaction of Figure 5a can be described by

$$F \underset{k_{red}'}{\overset{k_{ox}'}{\rightleftharpoons}} \dot{R}^+ \qquad (8)$$

Here, F denotes the fraction of the fluorophore molecules within the detection volume that are in a fluorescently viable, non-ionized state. On the time scale of the reaction, they have an average fluorescence brightness, which is proportional to the steady-state population of the first-excited singlet state and based on the steady-state populations of the singlet and triplet states. $\dot{R}^+$ is the fraction of photoionized, nonfluorescent, fluorophores. k_{ox}' and k_{red}' are the effective rates of photoionization and reduction of photoionized fluorophores, respectively.

In previous studies of photobleaching by FCS, the quantum yield of photobleaching, Φ_b, defined as

$$\Phi_b = \frac{\text{number of photobleached molecules}}{\text{total number of absorbed photons}} \qquad (9)$$

was found to increase with higher excitation intensities, in particular at levels at or close to excitation saturation, $I_{sat} = k_{10}/\sigma_{01}$.[9,12] Here, k_{10} is the deactivation rate of the first-excited singlet state S_1 to the ground singlet state S_0, and σ_{01} denotes the excitation cross section from S_0 to S_1. This increase of Φ_b was found to be taken well into account by including excitation to higher excited singlet and triplet states from which a subsequent photobleaching reaction may occur. The inclusion of higher excited singlet and triplet states also is supported by pulse radiolysis studies in which excited-state absorption of Rhodamine dyes was found to be significant over a broad range of visible excitation wavelengths,[49] and photoionization could be recorded following both mono- and bi-photonic absorption.[49−51]

For the photoionization occurring in our experiments, we therefore take the population of (and photoionization from) higher excited singlet and triplet states of Rh6G into account by use of a 5-state model (Figure 5b), including S_0 and S_1, the *n*th excited singlet state S_n, and their corresponding triplet states, T_1 and T_n. On the time scale of photoionization/reduction, we can restrict ourselves to consider only the steady-state populations of the states within this 5-state model:[12]

$$S_{0eq} = \frac{k_{Tn1}k_{Sn1}k_T k_{10}}{k_{Tn1}k_T(k_{Sn1}(k_{10}+k_{01})+k_{01}k_{S1n})+k_{ISC}k_{Sn1}k_{01}(k_{T1n}+k_{Tn1})}$$

$$S_{1eq} = \frac{k_{01}}{k_{10}}S_{0eq}$$

$$T_{1eq} = \frac{k_{ISC}}{k_T}S_{1eq} \qquad (10)$$

$$S_{neq} = \frac{k_{S1n}}{k_{Sn1}}S_{1eq}$$

$$T_{neq} = \frac{k_{T1n}}{k_{Tn1}}T_{1eq}$$

The rate coefficients are defined in Figure 5b with the excitation rate from S_0, S_1, and T_1 given by the excitation cross sections from the state in question as $k_{01} = \sigma_{01}I_{exc}$, $k_{S1n} = \sigma_{S1n}I_{exc}$ and $k_{T1n} = \sigma_{T1n}I_{exc}$, respectively. In this model, as an approximation we disregard intersystem crossing involving S_n and T_n, because the deactivation rates k_{Sn1} and k_{Tn1} have been reported to be of the order 5×10^{12} s^{-1} [12] leading to corresponding low quantum yields of intersystem crossing. From eq 10, it can be seen that the I_{exc}-dependence of S_{1eq} and S_{neq} differ only by a scaling factor from that of T_{1eq} and T_{neq}, respectively. We therefore only consider the joint contribution from both T_{1eq} and S_{1eq} to the effective rate of photoionization on the one hand, and that of T_{neq} and S_{neq} on the other. In other words, we assume that the effective rate of photoionization, k_{ox}', is proportional to and takes place by equal rates, k_{ox1} and k_{oxn}, from T_{1eq}/S_{1eq} and T_{neq}/S_{neq}, respectively:

$$k_{ox}' = k_{ox1}[S_{1eq}+T_{1eq}] + k_{oxn}[S_{neq}+T_{neq}]$$
$$k_{red}' = k_{red}[nPG] \qquad (11)$$

Here, the effective rate of reduction of $\dot{R}^+$, denoted k_{red}', is assumed to depend on the rate of collisional interactions of $\dot{R}^+$ with nPG and to be proportional to the nPG concentration by the bimolecular rate constant $k_{red}' = k_{red}[nPG]$. With reference to eq 4, we introduce the relaxation time of photo-oxidation/reduction, τ_R, and the probability of finding the flurophores in the detection volume in a photo-oxidized state, $\dot{R}^+$ replacing $1/k_B$ and B respectively:

$$\tau_R = \frac{1}{k_B} = \frac{1}{k_{red}' + k_{ox}'} \qquad (12)$$

$$\dot{R}^+ = B = \frac{k_{ox}'}{k_{red}' + k_{ox}'} \qquad (13)$$

To test this model more in detail, τ_R and $\dot{R}^+$ were measured systematically by FCS for a range of nPG concentrations (0.1−20 μM) and excitation intensities (10−1500 kW/cm^2). For each nPG concentration, the pair of τ_R and $\dot{R}^+$, measured at more than 10 different excitation intensities, were globally fitted to the expressions of eqs 12 and 13 (incorporating eqs 10 and 11) by variation of the parameters k_{ox1}, k_{oxn} and k_{red}'. In the fitting procedures, and in the calculation of the steady-state populations of the electronic states of Figure 5b from eq 10, σ_{01} and k_{10} were fixed to 2.22×10^{-16} cm^2 and 250×10^6 s^{-1}, and k_{ISC} and k_T to 1.1×10^6 s^{-1} and 0.49×10^6 s^{-1}, respectively.[8] Further, for the excitation to the higher singlet and triplet states, the literature values $\sigma_{Sn1} = 0.077 \times 10^{-16}$cm^2 and $\sigma_{Tn1} = 0.38 \times 10^{-16}$cm^2 were used.[52] The rates of k_{Sn1} and k_{Tn1} were set to 5×10^{12} s^{-1} [12] in agreement with earlier determinations of these rate constants for Rh6G[53] and for other xanthene dyes[54] in water. The fitted expressions for τ_R and $\dot{R}^+$, together with their corresponding experimental values, plotted versus the applied excitation intensities at [nPG] = 0.2, 1, 5, and 20 μM are included in Figure 6, panels a−d. The parameters of k_{ox1}, k_{oxn} and k_{red}' obtained after fitting the experimental parameters obtained from each concentration of nPG are plotted versus [nPG] in Figure 7. While k_{ox1} and k_{oxn} remain close to constant and independent of [nPG], k_{red}' shows a linear dependence from which a slope of $k_{red} = 2.3 \times 10^9$ M^{-1} s^{-1} can be determined. We note that k_{red} has an intermediate value in relation to k_{ass0} and k_{ass1} in Figure 3, and that the transfer of electrons from nPG to Rh6G thus takes place with about equal efficiency; either the Rh6G molecule is in its cation radical state (k_{red}) or in S_0 (k_{ass0}, inset Figure 2) or S_1 (k_{ass1}, inset Figure 2). From Figure 7, k_{ox1} and k_{oxn} can be estimated to average values of 2×10^3 and 0.8×10^9 s^{-1}, respectively. It should be noted that in the determination of k_{oxn}, k_{Sn1} and k_{Tn1} were fixed to literature values, which can be inaccurate by at least a factor of 2. Therefore, k_{oxn} should rather be considered as ratios $k_{oxn}/k_{Sn1} = k_{oxn}/k_{Tn1} = 1.6 \times 10^{-4}$, i.e., as photoionization pre-factors to the cross-sections σ_{S1n} and σ_{T1n}, or in other words, as the photoionization quantum yields, $\Phi(S_n)_{ion}$ and $\Phi(T_n)_{ion}$, of S_n and T_n, respectively. The corresponding photoionization quantum yield of S_1 is $\Phi(S_1)_{ion} = k_{ox1}/k_{10} = 0.8 \times 10^{-6}$. From eqs 10 and 11, a composite photoionization quantum yield of S_1 and T_1 can be defined as: $\Phi(S_1,T_1)_{ion} = \Phi(S_1)_{ion}[1 + k_{ISC}/k_T] = 2.6 \times 10^{-6}$. For low excitation intensities, when excitation to higher singlet and triplet states can be neglected, $\Phi(S_1,T_1)_{ion}$ can be considered as the photoionization analogue of Φ_b for photobleaching (eq 9). The difference of 2 orders of magnitude between $\Phi(S_1)_{ion}$ and $\Phi(S_n)_{ion}$ is well in agreement with previous findings by flash photolysis showing that ionization can be both mono and biphotonic with a considerably higher ionization yield following after biphotonic excitation.[24,50,51]

4.1.3. Ascorbic Acid in Water. The dependence of k_{ox1}, k_{oxn}, and k_{red}' on [nPG] (Figure 7) and the dependence of τ_R and $\dot{R}^+$ on I_{exc} for each [nPG] (Figure 6) well support the hypothesized model of photo-oxidation and subsequent restoring reduction of the photo-oxidized fluorophores by nPG, taking place via collisional interactions. To strengthen the support of the model further, we also investigated the response on the measured τ_R and $\dot{R}^+$ after addition of the well-known antioxidant AA in similar concentrations and under similar excitation conditions.

As for the investigation involving nPG, a series of correlation curves of Rh6G in water were recorded at different AA concentrations and excitation intensities using an expanded volume element. The results are very similar to those obtained after addition of nPG. As shown in Figure 8, addition of increasing amounts of AA in the submillimolar concentration range to the Rh6G solution increases the overall correlation

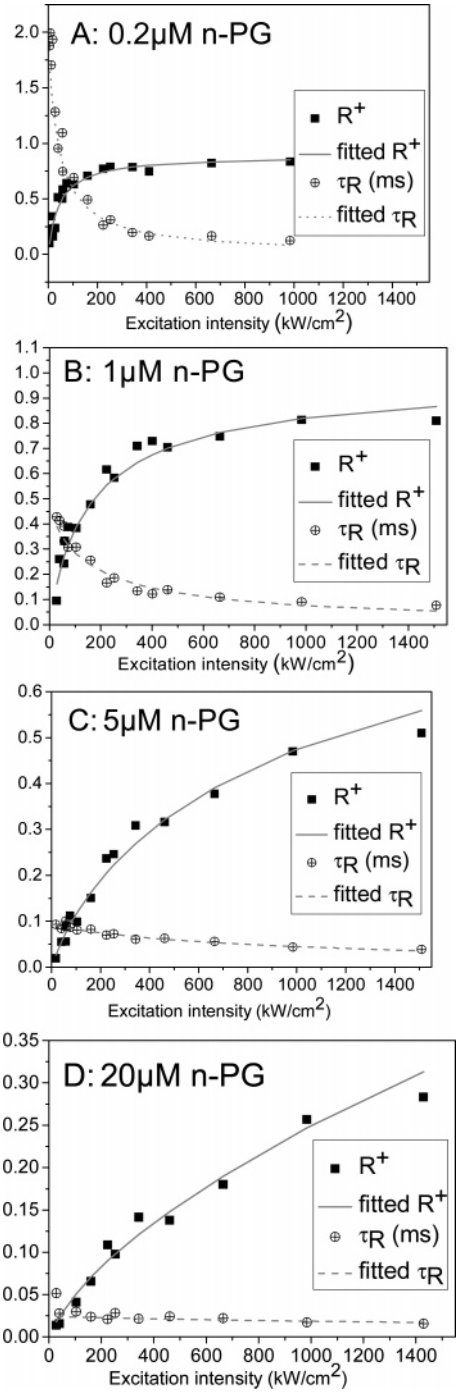

Figure 6. (A−D): Relaxation times for photo-oxidation/reduction, τ_R (replaces $1/k_B$ in eq 4), and the fraction of fluorophores being in a photo-oxidized state, $\dot{R}^+$ (replaces B in eq 4), determined by FCS at different excitation intensities for the nPG in aqueous solution at concentrations 0.2, 1, 5, and 20 μM. The fitted expressions for τ_R (eq 12) and $\dot{R}$;$\ddot{R}^+$ (eq 13) are for each concentration indicated by a dashed and a solid line, respectively.

decay time. As for nPG, the measured τ_R and $\dot{R}^+$ agree well with the schedule of Figure 5b. Global fitting of the measured τ_R and $\dot{R}^+$ parameters, recorded at different excitation intensities, yielded $k_{ox1} = 4 \times 10^3$ s^{-1}, $k_{oxn} = 0.6 \times 10^9$ s^{-1}, and $k_{red} = 1.3 \times 10^9$ M^{-1} s^{-1}. Our observations of the influence of nPG and AA on Rh6G are well in line with the reported oxidation potentials of AA (0.86 V versus NHE in H_2O) and nPG (0.82 V versus NHE in 4:96 MeOH/H_2O).[55] The somewhat lower k_{red} of AA compared to that of nPG can be a consequence of the

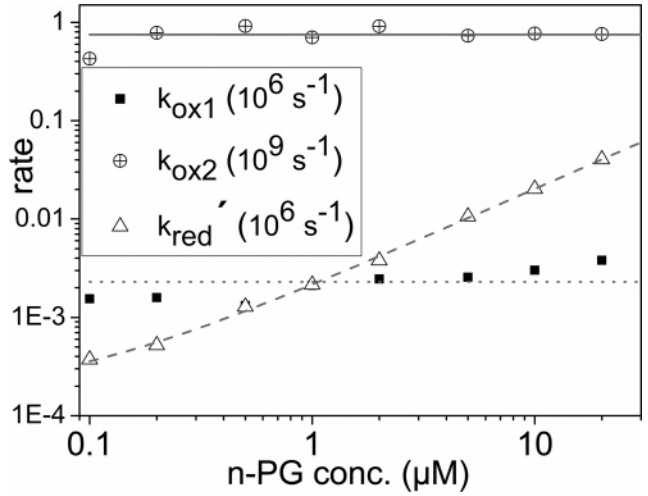

Figure 7. The parameters of k_{ox1}, k_{oxn}, and k_{red}' obtained after fitting the experimental parameters obtained from each concentration of nPG (Figure 6a−d). Linear regression analysis on the k_{red}' values yields the slope $k_{red} = 2.3 \times 10^9$ M^{-1} s^{-1}. k_{ox1} and k_{oxn} show an [nPG]-independent behavior with $k_{ox1} = 2.1 \times 10^3$ s^{-1} and $k_{oxn} = 8 \times 10^8$ s^{-1}.

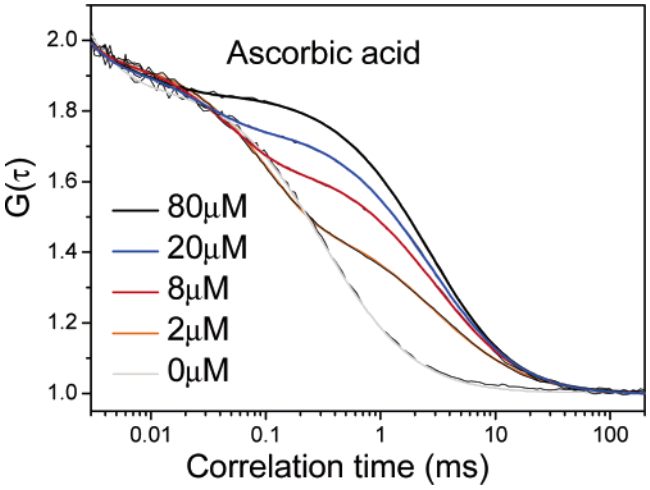

Figure 8. FCS curves of Rh6G in aqueous solution with different concentrations of ascorbic acid added (2−80 μM). Excitation intensity 0.7 MW/cm^2. $\dot{R}^+/\tau_R$ values of the curves: 0.13/0.009 ms (80 μM), 0.20/0.026 ms (20 μM), 0.32/0.49 ms (0.5 μM), 0.76/1.6 ms (0 μM). $T_{eq} = 0.16 \pm 0.01$ and $\tau_T = 2.3 \pm 0.4$ μs for all curves. For reference, a correlation curve is added and measured at the same excitation intensity with no AA added. (Curves normalized to an amplitude of 1 at $\tau = 3$ μs).

AA molecules being less hydrophobic, and therefore less readily forming complexes with Rh6G. Given the relatively similar redox potentials reported in literature for AA and nPG, a less favorable matching of the redox-potentials between AA and $\dot{R}h6G^+$ (1.22V versus NHE in dimethylformamide) for electron transfer does not appear to be the dominating reason. The similar rates of electron transfer induced fluorescence quenching (k_{ass0} and k_{ass1}) that we observe for nPG, and that which has been measured previously for dGTP, indicate that the quenching rates for both compounds are close to diffusion controlled.

4.1.4 Summary of Observed Effects of Antioxidants. From the effects of nPG and AA on the fluorescence of Rh6G, it seems as if the concentration of antioxidants has to be balanced. With reference to the scheme outlined below (eq 14, combining the schemes of eqs 6 and 8), we note that antioxidants can bring photo-oxidized dye species, $\dot{R}^+$ back to a fluorescent form F (within which transitions between the singlet and triplet states can take place). The antioxidants then have to be present at

high enough concentrations that the effective rate of reduction, k_{red}', can compete with the effective photo-oxidation rate, k_{ox}'. On the other hand, if present at too high concentrations, the extent of reduction of fluorescent dye molecules by the antioxidants can get significant and can generate a strong static as well as dynamic quenching. This reduction is effectuated by the effective rate of reduction following association, k_{ass}', in eq. 6.

$$C \underset{k_{diss0}}{\overset{k_{ass}'}{\rightleftarrows}} \boxed{S \underset{k_T}{\overset{k_{ISC}'}{\rightleftarrows}} T_1}_{F} \underset{k_{red}'}{\overset{k_{ox}'}{\rightleftarrows}} \dot{R}^+ \qquad (14)$$

In contrast to previous reports, our observations indicate that the quenching effects at high concentrations of antioxidants seem only to a very minor extent to be related to an increase of triplet state populations and then only indirectly. This indirect increase can follow as an effect of decreased accessibility of oxygen molecules to the dye molecules when in complex with the antioxidant molecules.[15] For both nPG and AA, a slight increase of k_{ox1} for concentrations above 5−10 μM could be observed (Figure 7). The reason for this increase is not fully clear. One possibility is that it is due to interference with the triplet state kinetics. With higher concentrations (>5−10 μM) the relaxation times of ionization/reduction (τ_R) start to partially overlap with those of singlet−triplet transitions (τ_T), and although separable the fitted parameters from the two relaxation processes may systematically influence each other. The obtained values for k_{ox1} and k_{oxn}, and their corresponding photoionization quantum yields are relatively well in agreement with the corresponding values for photobleaching in our previous FCS studies.[9,12] It is therefore reasonable to believe that, at least within the time scale of the translation of the fluorescent molecules through the detection volume of FCS (typically <10 ms), photoionization is the major mechanism of photodegradation. On the other hand, the photoionization seems to be almost fully recoverable at least by addition of antioxidants.

4.2. Addition of Triplet State Quenchers. *4.2.1. MEA in Aqueous Solution.* Adding MEA into an aqueous solution of Rh6G led to a clear reduction of the triplet state contribution in the correlation curves (Figure 9a). Moreover, in addition to the triplet state relaxation (~1 μs range), an additional relaxation process in the ~10 μs range could be observed (Figure 9a) with an amplitude that increased with the applied excitation intensities. By fitting the correlation curves measured at different excitation intensities to eq 5 (eq 1 with an additional exponential relaxation process) and then fitting all the obtained τ_T and T_{eq} at different excitation intensities but with the same concentration of MEA to eqs 2 and 3, respectively, the rates for intersystem crossing k_{ISC} and triplet state decay k_T could be determined. This fitting procedure was done as described in ref 8, also taking into account effects of nonuniform excitation within the detection volume. The triplet state rate parameters determined for different concentrations of MEA are plotted in the inset of Figure 9a as functions of MEA concentration. It can be seen that k_T increases linearly with the MEA concentration ($k_T = 0.5 \times 10^6\ s^{-1} + 0.9 \times 10^9\ M^{-1}\ s^{-1}$ [MEA]) while k_{ISC} remains essentially unaffected (on average $1.2 \times 10^6\ s^{-1}$). Population of triplet states, or other photoinduced states with low quantum yields of formation but with long lifetimes, can be quite significant in FCS measurements in which excitation intensities close to the saturation limit are often applied. In agreement with this, we observe that addition of MEA to an air-saturated aqueous Rh6G solution can produce a strong increase in the

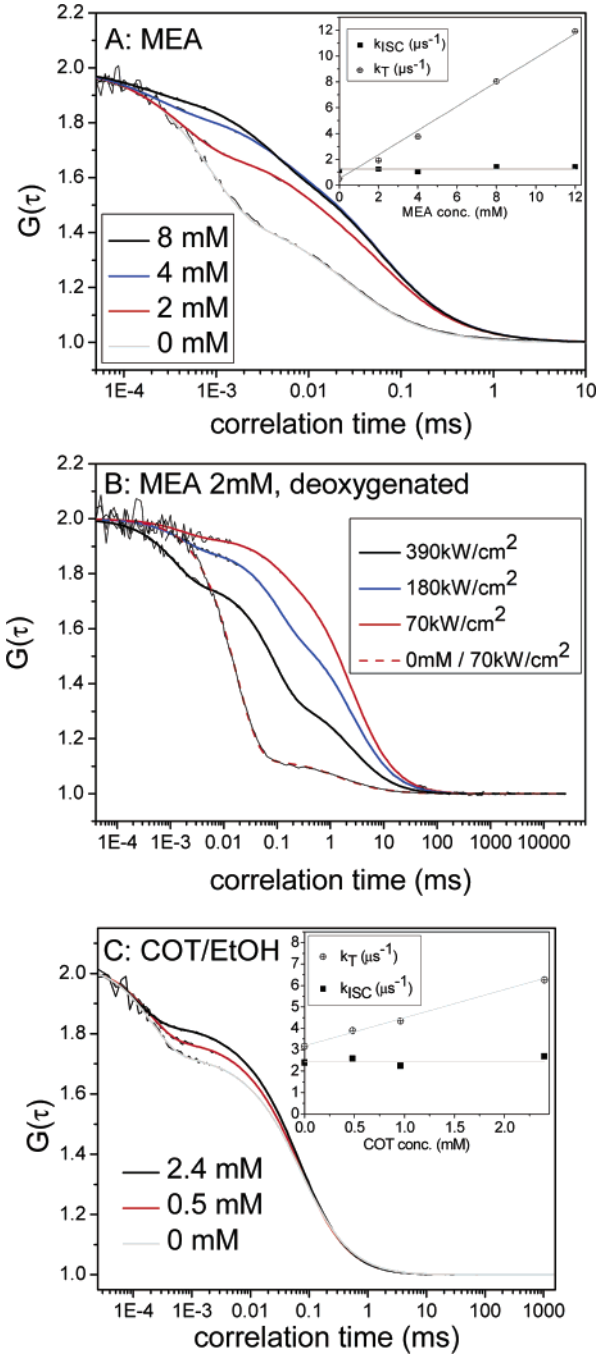

Figure 9. (A): FCS curves of Rh6G in aqueous solution with addition of MEA at different concentrations (0−8 mM). Excitation intensity 2.9 MW/cm^2 for all correlation curves. For these curves, the fitted relaxation parameters according to eq 4 were (T/τ_T, B/τ_B): 0.089/0.14 μs, 0.27/3.4 μs (8 mM), 0.15/0.21 μs, 0.20/4.0 μs (4 mM), 0.30/0.40 μs, 0.19/7.7 μs (2 mM), 0.54/0.84 μs (0 mM, triplets only). Inset: the [MEA] dependence of k_{ISC} and k_T, extracted from FCS measurements and the τ_T and T_1, measured at different excitation intensities (10 kW/cm^2−3MW/cm^2). (B): FCS curves of Rh6G in deoxygenated aqueous solution with addition of 2 mM MEA at different excitation intensities. For these curves, the fitted relaxation parameters according to eq 4 were (T/τ_T, B/τ_B): 0.067/1.6 μs, 0.14/110 μs (70 kW/cm^2), 0.11/1.7 μs, 0.32/100 μs (180 kW/cm^2), 0.23/1.2 μs, 0.55/86μs (390 kW/cm^2), 0.88/17 μs (0 mM, triplets only). (C): FCS curves of Rh6G in ethanol with addition of COT at different concentrations (0−2.4 mM). Excitation intensity 1 MW/cm^2 for all correlation curves. For these curves, the fitted relaxation parameters according to eq 4 were (T/τ_T, B/τ_B): 0.20/0.12 μs, 0.05/3.9 μs (2.4 mM), 0.25/0.19 μs, 0.04/5.7 μs (0.5 mM), 0.30/0.22 μs (0 mM, triplets only). Inset: the [COT] dependence of k_{ISC} and k_T, extracted from FCS measurements, and the τ_T and T_1 measured at different excitation intensities (40 kW/cm^2−2.2 MW/cm^2).

fluorescence count-rate per molecule, CPM, of approximately 100% (the CPM calculated as the product of the amplitude of the FCS curve after triplet state relaxation (equals 1/*N*, see eq 1) and the fluorescence count-rate registered during the FCS measurement). As the measurements indicate, this increase in fluorescence CPM is also observed in FCS measurements using a small detection volume in which the fast passage of the molecules reduces the effects of possible photobleaching. Our observations are well in agreement with previous investigations in which MEA has been reported to quench the triplet state of fluorescein without quenching the fluorescence.[5]

However, when increasing the concentrations of MEA above 2−6 mM, no significant further increase in the fluorescence output could be noticed. We attribute this to the process underlying the additional exponential relaxation process that could be observed in the FCS curves upon addition of MEA (Figure 9a). The relaxation rates of this process were somewhat lower than those of the singlet−triplet transitions and increased with higher excitation intensities (ranging from 1−5 μs (at 70 mM MEA and 200 kW/cm^2) and exceeding 1−200 μs at MEA concentrations in the sub-mM range). For MEA concentrations above 2−6 mM, the amplitude and the relaxation rate of this exponential process increased with the applied MEA concentrations (Figure 9a). On the other hand, for MEA concentrations below this range we instead noted decreasing relaxation amplitudes with increasing MEA concentrations. Overall, we attribute this process to MEA-induced reduction of the Rh6G molecules. This is in agreement with transient state absorption studies in which MEA has been found to quench radical forms of the dye fluorescein.[5]

For [MEA] > 2−6 mM, MEA preferentially reduces intact fluorescent Rh6G molecules. Here, MEA promotes the generation of a nonfluorescent, reduced form of Rh6G, and the amplitude of the relaxation process in the FCS curves consequently increases with the applied MEA concentration. (In analogy to nPG and with reference to eq 14, *C* increases at the expense of *F* due to an increased k_{ass}', which exceedes k_{diss0}). On the other hand, at lower concentrations MEA preferentially promotes the regeneration of photo-oxidized Rh6G into fluorescently viable Rh6G molecules in agreement with the observed decrease of the relaxation amplitude with increasing MEA concentrations (and analogous to a decrease of $\dot{R}^+$, due to an increased k_{red}' rate exceeding that of k_{ox}' (eq 14)). Overall, these effects of MEA in principle seem to be very similar to those observed for nPG (see sections 4.1.1. and 4.1.2.). However, given the slower relaxation times observed in the samples containing MEA, compared to samples with similar added concentrations of nPG, the reduction of Rh6G by MEA seems to be less efficient.

The relative effect of triplet state quenching of MEA in deoxygenated solutions is shown in Figure 9b. Molecular oxygen is believed to play an important role in photodegradation of fluorophores. On the other hand, oxygen is also an efficient triplet state quencher, and collisionally induced triplet state quenching by oxygen is the main contribution to k_T under air saturated conditions.[8,57] In principle, from a photostability point of view, it would be ideal to remove the oxygen and replace its triplet quenching effect by the addition of another triplet state quencher. After deoxygenation, we observe a strong accumulation of the fluorophores in their triplet states, which after addition of MEA indeed is strongly reduced (Figure 9b). However, we also found the amplitude of the second relaxation process in the FCS curves to be more prominent (2−3 times higher) in deoxygenated aqueous solutions compared to air-saturated solutions at similar excitation intensities and MEA concentrations (Figure 9b). Also, the relaxation times of this process were found to be longer. This is well in agreement with previous reports stating that the major decay pathway of the reduced, nonfluorescent form of Rh6G is by collisional interactions with molecular oxygen.[57] From this point of view, addition of MEA to deoxygenated solutions has a stronger relative effect on the triplet state population. However, MEA also promotes formation of reduced Rh6G, which in the absence of oxygen can be strongly accumulated. Therefore, in deoxygenated as well as in air-saturated solutions, there is for MEA a tradeoff between triplet quenching on the one hand and fluorophore reduction on the other. Typically, efficient triplet state quenching only seems to be effectuated at MEA concentrations in which a significant population of the nonfluorescent reduced form of Rh6G is also generated, irrespective of the oxygen concentration of the aqueous solution.

4.2.2. COT in Ethanol. In Figure 9c, FCS curves for Rh6G in ethanol with different concentrations of COT are shown. It can clearly be seen that COT diminishes the degree of triplet state build up. The effect of COT in ethanol was analyzed in the same way as MEA in aqueous solution. Similarly, the intersystem crossing rate, k_{ISC}, remained the same at different COT concentrations, while the triplet decay rate increased linearly with the COT concentration (see inset Figure 9c). At concentrations above approximately 3 mM, the triplet quenching effect of COT was diminished probably because of micelle formation of the COT molecules.[38] Below this limit, the addition of COT enhanced the fluorescence output from the Rh6G molecules. The maximum CPM increased by almost 100% upon addition of COT. These results support the view of COT as a potent triplet state quencher of Rh6G and other laser dyes as put forth by investigators more than 30 years ago[39−41] and disfavor a somewhat more recent idea that COT exerts its beneficial effect on lasing by retarding the k_{ISC} of the dyes.[38] As with MEA in aqueous solution, a second exponential process could be identified in the correlation curves recorded for Rh6G with COT/EtOH. However, at comparable excitation intensities and COT concentrations the relative amplitudes of this second relaxation process, and thus the populations of the corresponding transient, nonfluorescent form of Rh6G, were almost an order of magnitude lower than for MEA/H_2O. This relaxation time possibly can be attributed to an electron transfer process. However, because of the low relative amplitudes observed for this process and the reported complex redox properties of COT,[58] the identity of this relaxation process was not further investigated.

5. Optimization of Fluorescence Output Per Molecule in an Expanded Detection Volume

In Figure 10, panels a and b, the effects of addition of nPG and MEA at different concentrations on the fluorescence count-rate per molecule (CPM) of Rh6G is plotted as a function of excitation intensity, recorded in an expanded laser beam/detection volume (ω_0 = 1.2 μm, pinhole diameter =150 μm, objective: 60x, 1.2 NA). In agreement with previous findings, addition of the antioxidant nPG in micromolar concentrations has a strongly beneficial effect on the recorded CPM. However, at increased concentrations the extent of electron donation and quenching of intact fluorophores by the antioxidants becomes increasingly dominant and reduces the fluorescence brightness of the fluorophores. An optimum in CPM is reached at concentrations where k_{red}' is comparable to or higher than k_{ox}' and where k_{ass0} and k_{ass1} are still close to negligible compared

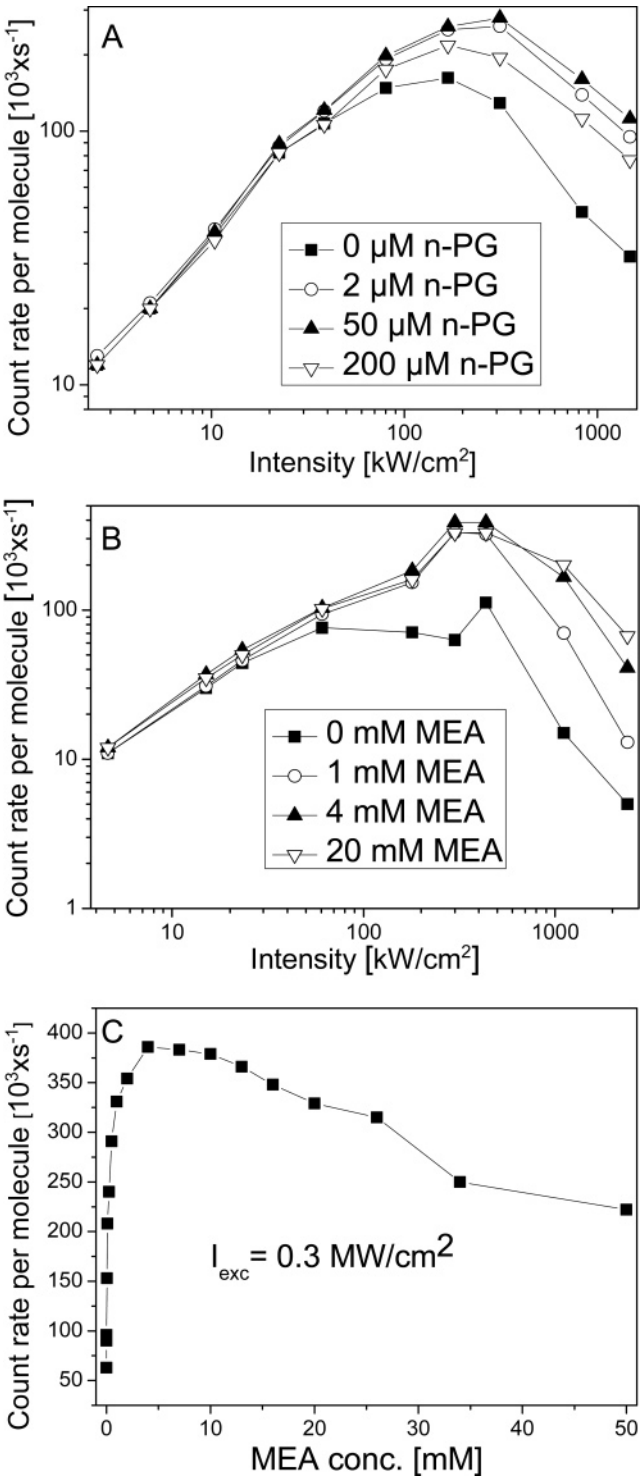

Figure 10. (A−B): CPM of Rh6G measured by FCS with an expanded volume element ($\omega_0 = 1{,}2\ \mu$m, pinhole diameter = 150 μm, objective: 60x, 1.2 NA) versus excitation intensity and after addition of different concentrations of MEA (A) and nPG (B). (C): CPM of Rh6G measured in the same experimental setup at an excitation intensity of 0.3 MW/cm^2, as a function of added concentration of MEA.

to k_{diss0}. With reference to eq 14, the useful concentration interval of an added antioxidant can thus be defined as:

$$k_{ox}'/k_{red} < [\text{antioxidant conc.}] < k_{diss0}/k_{ass}' \qquad (15)$$

For both nPG and AA acting on Rh6G in aqueous solution, the optimum is found already at a concentration of about 2 μM (Figure 10a). Typically, no significant additional gain in CPM can be noticed for higher concentrations, except at excitation intensities close to or above several hundreds of kW/cm^2. At these intensities, k_{ox}' is prominent, and the beneficial effects of nPG and AA on k_{red}' can still dominate over the likewise strong quenching effects, effectuated by k_{ass0} and k_{ass1}. However, at these excitation intensities the antioxidative effect can still by far compensate the overall photo-oxidation/photobleaching, and the recorded CPM is considerably less than the optimum CPM of about 300 kHz, obtained at 200−300 kW/cm^2.

After addition of MEA (Figure 10, panels b and c) even higher CPMs (up to 400 kHz) can be obtained than for AA or nPG. To some extent, this reflects the double impact of triplet state quenching. On the one hand, by reduction of T_{1eq} itself, the average fluorescent brightness of the (non photo-oxidized) fluorophores increases. In addition, the population of a possible precursor state of photo-oxidation/photobleaching is reduced, thereby leading to a lower rate of photodegradation. However, as mentioned above, we also noted the presence of an additional relaxation process in the FCS curves, which we attribute to electron transfer from MEA to Rh6G and reduction/quenching of the Rh6G molecules (Figure 9a). In analogy to the effects of the antioxidants AA and nPG, this electron transfer can also possibly work advantageously in particular at excitation intensities at or close to saturation, regenerating photo-oxidized fluorophores into fluorescently viable states by reduction. This combined effect of reduction and triplet quenching can explain the higher maximum count rates obtainable with MEA, compared to those reached after addition of AA or nPG. As judged from the CPM dependence of the MEA concentration and the applied excitation intensities (and similar to the effects of AA and nPG), the effects of the reduction of photo-oxidized states dominates over the reduction/quenching of nonphoto-oxidized states at lower MEA concentrations. The overall maximum count rates are reached at $I_{exc} = 200-300$ kW/cm^2 with approximately 4 mM of MEA. It is interesting to note that the optimum MEA concentration is considerably lower than that required for a full triplet quenching (Figure 9a). This indicates that for MEA, its antioxidative properties and the balance between electron donation to photo-oxidized fluorophores (promoting fluorescence) and the reduction of non photo-oxidized fluorophores (quenching fluorescence) is at least as important as the extent of triplet quenching. In other words, the MEA concentration at which an optimum CPM was obtained is strongly determined by the antioxidative properties of MEA. This conclusion is further supported by the observation that the addition of antioxidants (AA or nPG) to a solution of MEA at optimum concentrations (∼4 mM) led to a clear reduction of CPM for Rh6G (except at I_{exc} far above the overall CPM maximum).

6. Concluding Remarks

Photostability and fluorescence brightness per fluorescent molecule (reflected in the CPM) remain prime figures of merit for virtually all ultrasensitive fluorescence spectroscopic techniques, such as FCS and SMD, but also for a range of applications of fluorescence spectroscopy in which a high read out rate is required. In this paper, we have defined and characterized mechanisms that retard photobleaching and enhance fluorescence in such measurements based on triplet state quenchers and antioxidants. We note that within typical transit times of fluorescent molecules through the detection volume in a confocal FCS or SMD instrument (<10−20 ms), prominent photoionization and dye radical formation can occur. At excitation intensities at or close to saturation, photoionization

from higher excited singlet and triplet states contribute significantly to the overall rate of photoionization. Our results confirm previous reports identifying radical formation as an important process involved in photobleaching. This study also confirms the reported positive effects of antioxidants, reducing photoionized fluorophores back into their fluorescently viable states.[26,29,34,36,37,59] Moreover, it identifies the balance between reduction of photoionized fluorophores and that of intact fluorophores as an important guideline for what concentration of an antioxidant to be added for optimal fluorescence generation in FCS and SMD experiments. It is interesting to note that the optimal concentration for nPG/AA to act on Rh6G in an aqueous solution was found to be in the lower micromolar range, which is considerably lower than what previously has been suggested. The optimal concentration depends on the excitation intensity and can be expected to vary depending on the combination of fluorophore/antioxidant. For fluorophores with higher photooxidation yields than that of Rh6G, it is reasonable to assume that considerably higher concentrations of antioxidants are needed to avoid a strong build up of photo-oxidized fluorophores. The range of useful concentrations of an added antioxidant, as defined in eq 15, thus can be shifted to higher concentration ranges, can be more narrow, or may even be impossible to define (if the antioxidant concentration needed to yield a k_{red} that can counterbalance a high k_{ox}' also generates a prominent k_{ass}'). For Rh6G and other dyes with similar photooxidation yields, the need to add less concentration of antioxidants than previously anticipated should also lead to a reduced perturbation of the molecules/biological system under study. Also, for MEA, a compound termed as a triplet state quencher, it is in the end its antioxidative properties and the balance between reduction of fluorophore cation radicals and intact fluorophores that defines the optimal concentration. Interestingly, at this optimal concentration, the triplet state quenching is far from sufficient to fully minimize the triplet populations.

Finally, apart from being a process that needs to be characterized to optimize fluorescence output in fluorescence experiments, the fluorescence blinking caused by the photoionization/reduction cycle may be taken advantage of. The monitoring of electron transfer by FCS has been demonstrated to provide an interesting approach for biomolecular dynamic and structural studies.[15,60] From that point of view, it is interesting to note that this study demonstrates that the electron donation from one and the same antioxidant/fluorophore pair can switch fluorescence either on or off and can thus be conveniently monitored by fluctuation analysis over a broad concentration range at time scales from nanoseconds up to milliseconds or seconds. In fluorescence microscopy, efficient switching of fluorophores to and from a photoinduced state has proven to offer an exciting means to reach ultrahigh resolution by visible light, far beyond the diffraction limit.[61,62] The photoionization/reduction cycle, as characterized and controlled in this study, may provide a new attractive mechanism to be used in these contexts, offering a high contrast in fluorescence brightness, a large flexibility and tunability in population kinetics, induced by only minor environmental changes.

Acknowledgment. This study was supported by the Swedish Research Council (VR−NT), the Swedish Strategic Research Foundation (SSF-BioX), the European 6th Framework Programme (SPOTLITE), and the Swedish Foundation for Internationalization of Higher Education and Research (STINT, Institutional Grant). C.S. gratefully acknowledges the financial support by the BMBF Biofuture Grant 0311865 and the SFB 663, Heinrich Heine Universität. C.E. acknowledges support from BMBF Grant 0312020A. We thank Professor Theo Lasser, EPFL, Lausanne, and Daniela Pfiffi, Heinrich-Heine Universität, Düsseldorf, for valuable comments on the manuscript.

References and Notes

(1) Tsien, R. Y.; Waggoner, A. Fluorophores for Confocal Microscopy - Photophysics and Photochemistry. In *Handbook of Biological Confocal Microscopy*; 2nd ed.; Pawley, J. B., Ed.; Plenum Press: New York, 1995; pp 267.
(2) Longin, A.; Souchier, C.; French, M.; Bryon, P. A. *J. Histochem. Cytochem.* **1993**, *41*, 1833.
(3) Hirschfeld, T. *J. Histochem. Cytochem.* **1979**, *27*, 96.
(4) Bernas, T.; Zarebski, M.; Dobrucki, J. W.; Cook, P. R. *J. Microsc.* **2004**, *215*, 281.
(5) Song, L.; Varma, C. A.; Verhoeven, J. W.; Tanke, H. J. *Biophys. J.* **1996**, *70*, 2959.
(6) Bock, G.; Hilchenbach, M.; Schauenstein, K.; Wick, G. *J. Histochem. Cytochem.* **1985**, *33*, 699.
(7) Florijn, R. J.; Slats, J.; Tanke, H. J.; Raap, A. K. *Cytometry* **1995**, *19*, 177.
(8) Widengren, J.; Mets, Ü.; Rigler, R. *J. Phys. Chem.* **1995**, *99*, 13368.
(9) Widengren, J.; Rigler, R. *Bioimaging* **1996**, *4*, 149.
(10) Usui, Y.; Itoh, K.; Koizumi, M. *Bull. Chem. Soc. Jpn.* **1965**, *38*, 1015.
(11) Benson, D. M.; Bryan, J.; Plant, A. L.; Gotto, A. M., Jr.; Smith, L. C. *J. Cell Biol.* **1985**, *100*, 1309.
(12) Eggeling, C.; Widengren, J.; Rigler, R.; Seidel, C. A. M. *Anal. Chem.* **1998**, *70*, 2651.
(13) Eggeling, C.; Widengren, J.; Brand, L.; Schaffer, J.; Felekyan, S.; Seidel, C. A. *J. Phys. Chem. A* **2006**, *110*, 2979.
(14) Widengren, J.; Rigler, R.; Mets, Ü. *J. Fluoresc.* **1994**, *4*, 255.
(15) Widengren, J.; Dapprich, J.; Rigler, R. *Chem. Phys.* **1997**, *216*, 417.
(16) Widengren, J.; Schwille, P. *J. Phys. Chem. A* **2000**, *104*, 6416.
(17) Talhavini, M.; Atvars, T. D. Z. *J. Photochem. Photobiol., A* **1999**, *120*, 141.
(18) Wilkinson, F.; Mcgarvey, D. J.; Olea, A. F. *J. Phys. Chem.* **1994**, *98*, 3762.
(19) Davidson, R. S. *Pestic. Sci.* **1979**, *10*, 158.
(20) Sanchez, E. J.; Novotny, L.; Holtom, G. R.; Xie, X. S. *J. Phys. Chem. A* **1997**, *101*, 7019.
(21) Eggeling, C.; Volkmer, A.; Seidel, C. A. M. *ChemPhysChem.* **2005**, *6*, 791.
(22) Harada, Y.; Sakurada, K.; Aoki, T.; Thomas, D. D.; Yanagida, T. *J. Mol. Biol.* **1990**, *216*, 49.
(23) Mei, E.; Tang, J. Y.; Vanderkooi, J. M.; Hochstrasser, R. M. *J. Am. Chem. Soc.* **2003**, *125*, 2730.
(24) Zondervan, R.; Kulzer, F.; Kol'chenko, M. A.; Orrit, M. *J. Phys. Chem.* A **2004**, *108*, 1657.
(25) English, D. S.; Furube, A.; Barbara, P. F. *Chem. Phys. Letters* **2000**, *324*, 15.
(26) van Dijk, M. A.; Kapitein, L. C.; van Mameren, J.; Schmidt, C. F.; Peterman, E. J. G. *J. Phys. Chem. B* **2004**, *108*, 6479.
(27) White, J. C.; Stryer, L. *Anal. Biochem.* **1987**, *161*, 442.
(28) Giloh, H.; Sedat, J. W. *Science* **1982**, *217*, 1252.
(29) Gaigalas, A. K.; Wang, L.; Cole, K. D.; Humphries, E. *J. Phys. Chem. A* **2004**, *108*, 4378.
(30) Panadero, S.; Gomezhens, A.; Perezbendito, D. *Analyst (Cambridge, U.K.)* **1995**, *120*, 125.
(31) Nakagawa, Y.; Nakajima, K.; Tayama, S.; Moldeus, P. *Mol. Pharmacol.* **1995**, *47*, 1021.
(32) Glazer, A. N. *FASEB J.* **1988**, *2*, 2487.
(33) Breidt, F. J.; Hayes, J. S.; McFeeters, R. F. *J. Food Prot.* **2004**, *67*, 12.
(34) Eggeling, C.; Widengren, J.; Rigler, R.; Seidel, C. A. Photostability of Fluorescent Dyes for Single-Molecule Spectroscopy. In *Applied Fluorescence in Chemistry, Biology, and Medicine*; Rettig, W., Strehmel, B., Schrader, S., Seifert, H., Eds.; Springer-Verlag: Berlin, Germany, 1999; pp 193.
(35) Vigers, G. P. A.; Coue, M.; McIntosh, J. R. *The J. Cell Biol.* **1988**, *107*, 1011.
(36) Dittrich, P. S.; Schwille, P. *Appl. Phys. B* **2001**, *73*, 829.
(37) Widengren, J. Photophysical aspects of FCS measurements. In *Fluorescence Correlation Spectroscopy, Theory and Applications.*; Rigler, R., Ed.; Springer-Verlag: Heidelberg, Germany, 2001; pp 276−300.
(38) Asimov, M. M.; Gavrilenko, V. N.; Rubinov, A. N. *J. Lumin.* **1990**, *46*, 243.
(39) Lüttke, W.; Schäfer, F. *Laser und Optoelektronik* **1983**, *2*, 127.
(40) Pappalardo, R.; Samelson, H.; Lempicki, A. *IEEE J. Quantum Electron.* **1970**, *6*, 716.
(41) Weber, J. *Opt. Commun.* **1973**, *7*, 420.

(42) Rigler, R.; Mets, Ü.; Widengren, J.; Kask, P. *Eur. Biophys. J.* **1993**, *22*, 169.
(43) Marquardt, D. W. *J. Soc. Ind. Appl. Math.* **1963**, *11*, 431.
(44) Magde, D.; Elson, E.; Webb, W. W. *Phys. Rev. Lett.* **1972**, *29*, 705.
(45) Elson, E. L.; Magde, D. *Biopolymers* **1974**, *13*, 1.
(46) Magde, D.; Elson, E. L.; Webb, W. W. *Biopolymers* **1974**, *13*, 29.
(47) Widengren, J.; Thyberg, P. *Cytometry* **2005**, *68A*, 101.
(48) Delon, A.; Usson, Y.; Derouard, J.; Biben, T.; Souchier, C. *J. Fluoresc.* **2004**, *14*, 255.
(49) Beaumont, P. C.; Johnson, D. G.; Parsons, B. J. *J. Chem. Soc., Faraday Trans.* **1998**, *94*, 195.
(50) Navaratnam, S.; Parsons, B. J. *J. Photochem. Photobiol., A* **2002**, *153*, 153.
(51) Ferguson, M. W.; Beaumont, P. C.; Jones, S. E.; Navaratnam, S.; Parsons, B. J. *Phys. Chem. Chem. Phys.* **1999**, *1*, 261.
(52) Thiel, E. Habilitation thesis, Universitat-GH Siegen, 1995.
(53) Ermolaev, V. L. *Opt. Spektrosk.* **1984**, *56*, 630.
(54) Penzkofer, A.; Beidoun, A. *Chem. Phys.* **1993**, *177*, 203.
(55) Diego, E.; Agui, L.; González-Cortez, A.; Yánez-Sedeno, P.; Pingarrón, J. M.; Kaufmann, J. M. *Electroanalysis* **1998**, *10*, 33
(56) Seidel, C; Schulz, A; Sauer, M *J. Phys. Chem.* **1996**, *100(13*), 5541
(57) Korobov, V. E.; Chibisov, A. K. *Usp. Khim.* **1983**, *52*, 43.
(58) Diego, E.; Agui, L.; González-Cortez, A.; Yánez-Sedeno, P.; Pingarrón, J. M.; Kaufmann, J. M. *Electroanalysis* **1998**, *10*, 33
(59) Widengren, J. Fluorescence correlation spectroscopy, photophysical aspects and applications, Dissertation, Karolinska Institutet, 1996.
(60) Neuweiler, H.; Schulz, A.; Bohmer, M.; Enderlein, J.; Sauer, M. *J. Am. Chem. Soc.* **2003**, *125*, 5324.
(61) Hell, S. W. *Nature Biotechnology* **2003**, *21*, 1347.
(62) Hofmann, M.; Eggeling, C.; Jakobs, S.; Hell, S. W. *Proc. Natl. Acad. Sci. U.S.A.* **2005**, *102(49*), 17565